

Group 3 Dialkyl Complexes of a Rigid Monoanionic NNN-Donor Pincer Ligand: Synthesis, Structures, Unexpected Reactivity with CPh_3^+ , and Hydroamination Catalysis

Received 00th January 20xx,
Accepted 00th January 20xx

DOI: 10.1039/x0xx00000x

Aathith Vasanthakumar,^a Novan A. G. Gray,^a Christopher J. Franko,^a Maia C. Murphy,^a David J. H. Emslie^{*a}

Palladium-catalyzed coupling of 4,5-dibromo-2,7,9,9-tetramethylacridan with two equivalents of 1,3-diisopropylimidazolin-2-imine afforded 4,5-bis(1,3-diisopropylimidazolin-2-imino)-2,7,9,9-tetramethylacridan, $\text{H}[\text{All}_2]$. Reaction of the $\text{H}[\text{All}_2]$ proligand with one equivalent of $[\text{M}(\text{CH}_2\text{SiMe}_3)_3(\text{THF})_2]$ ($\text{M} = \text{Y}$ or Sc) yielded the base-free neutral dialkyl complexes $[(\text{All}_2)\text{M}(\text{CH}_2\text{SiMe}_3)_2]$ ($\text{M} = \text{Y}$ (**1**) and Sc (**2**)). The rigid All_2 pincer ligand affords a similar steric profile to the previously reported XA_2 pincer ligand, but is monoanionic rather than dianionic. Reaction of **1** with one equiv. of $[\text{CPh}_3][\text{B}(\text{C}_6\text{F}_5)_4]$ in $\text{C}_6\text{D}_5\text{Br}$ generated a highly active catalyst for intramolecular alkene hydroamination. However, rather than forming the expected monoalkyl cation, this reaction afforded a diamagnetic product which was identified as $[(\text{All}_2\text{-CH}_2\text{SiMe}_3)\text{Y}(\text{CH}_2\text{SiMe}_3)_2][\text{B}(\text{C}_6\text{F}_5)_4]$ (**3**; $\text{All}_2\text{-CH}_2\text{SiMe}_3$ is a neutral tridentate ligand with a central amine donor flanked by imidazolin-2-imine groups) in approx. 20% yield, accompanied by HCPH_3 (~2 equiv. relative to **3**), an unidentified paramagnetic product (detected by EPR spectroscopy), and a small amount of colourless precipitate. The unexpected reactivity of **1** with CPh_3^+ is thought to involve initial All_2 ligand backbone oxidation, given that the zwitterionic form of the ligand contains a phenylene ring with two adjacent anionic nitrogen donors, similar to a redox-non-innocent, dianionic *ortho*-phenylenediamido ligand.

Introduction

Pincer ligands have been used to great effect in the development of late transition metal organometallic chemistry and homogeneous catalysis, and have recently seen increased application in early transition metal and f-element chemistry.¹⁻³ Within this class of ligand, those based on a tricyclic backbone composed of three 6-membered rings (e.g. anthracene, acridine, xanthene or acridan) can provide a particularly rigid coordination environment, and dianionic 4,5-bis(amido)-xanthene ligands (e.g. XA_2 and XN_2 ; Figure 1) have been shown to be highly effective for the isolation of reactive organometallic complexes. For example, our group has used the XA_2 and XN_2 dianions to prepare a range of thorium⁴⁻⁶ and uranium⁷⁻⁹ complexes, including non-cyclopentadienyl thorium and uranium alkyl cations¹⁰⁻¹² and a thorium dication,¹⁰ as well as a zirconium alkyl cation with high activity for ethylene polymerization,¹³ and neutral yttrium and lutetium monoalkyl complexes with high activity for intra- and intermolecular hydroamination.^{14,15} 4,5-Bis(amido)xanthene ligands with alkyl or terphenyl substituents on nitrogen have also been used to access organometallic titanium¹⁶ and uranium¹⁷ complexes, and

unique examples of potassium–alkane interactions.¹⁸ Furthermore, the XA_2 ligand was recently employed by Goicoechea and Aldridge *et al.* for the synthesis of an anionic aluminium(I) nucleophile, $[(\text{XA}_2)\text{Al}]^-$, which provided access to unique C–C and C–H bond activation chemistry,¹⁹⁻²¹ aluminium P_4^{2-} and P_4^{4-} complexes,²² coordination and homologation of CO at aluminium,²³ complexes featuring Al–Mg and Al–Li linkages,²⁴ reactive monometallic aluminium imide²⁵ and oxo²⁶ complexes, and a nucleophilic gold complex.²⁷ Copper, silver,^{28,29}

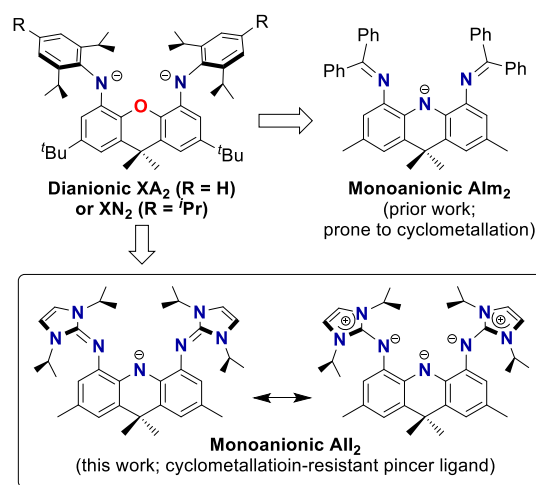


Figure 1. Relationship between the dianionic XA_2 ligand and the monoanionic Alm_2 and All_2 ligands.

^a Department of Chemistry and Chemical Biology, McMaster University, Hamilton, Ontario L8S 4M1, Canada.

Electronic Supplementary Information (ESI) available: NMR and EPR spectra, and graphs of % conversion vs time for hydroamination. See DOI: 10.1039/x0xx00000x. CCDC 2242707-2242708 contain the supplementary crystallographic data for **1** and **2**, respectively. These data can be obtained free of charge from The Cambridge Crystallographic Data Centre via www.ccdc.cam.ac.uk/data_request/cif.

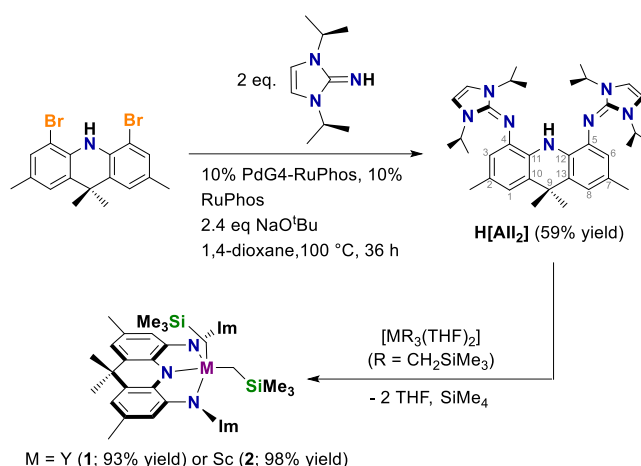
magnesium, calcium,³⁰ germanium, tin, and lead^{31,32} compounds were also reported. Furthermore, low-valent cobalt and iron complexes of a related 4,5-bis(silylamido)xanthene ligand were recently reported by the Tilley group, extending the chemistry of this ligand class to the late transition metals.³³

A limitation of 4,5-bis(amido)xanthene ligands is that their 2- charge does not allow for the synthesis of cationic alkyl complexes of the rare earth elements. Such cationic complexes are of interest as catalysts for alkene polymerization and hydroelementation, and would be accessible using a monoanionic analogue of the XA_2 ligand. One strategy to access such a ligand would be to switch from a neutral xanthene backbone with flanking anionic donors to an anionic acridanide backbone with flanking neutral donors (Figure 1). However, to maintain high rigidity analogous to that in XA_2 , the flanking donor atoms must be attached directly to the ligand backbone, and most applicable neutral donors do not exhibit cyclometallation resistance comparable to that of ubiquitous 2,6-diisopropylanilido donors. For example, in an initial foray into the synthesis of a monoanionic NNN-donor pincer ligand, we prepared the Alm_2 anion (Figure 1) with neutral $-\text{N}=\text{CPh}_2$ donors on an acridanide backbone. However, reaction with $[\text{Y}(\text{CH}_2\text{SiMe}_3)_3(\text{THF})_2]$ resulted in installation of two equivalents of the ligand, rather than one, and rapid cyclometallation.³⁴

As a more robust alternative, we envisaged a ligand featuring neutral 1,3-diisopropylimidazol-2-imine $\{-\text{N}=\text{Im}; \text{Im} = 1,3\text{-diisopropylimidazol-2-ylidene}\}$ donors³⁵⁻⁵¹ in the 4- and 5-positions of an acridanide backbone (All_2 ; Figure 1), where a zwitterionic resonance structure can be expected to allow the imidazole rings to lie perpendicular to the plane of the acridanide backbone, providing a steric profile similar of that of the XA_2 dianion (albeit with isopropyl groups slightly further removed from the metal coordination pocket due to their attachment in the *ortho* positions of a 5-membered rather than a 6-membered ring). Herein we describe the synthesis of the aforementioned All_2 ligand (as the protio ligand), alkane elimination reactions to afford room temperature-stable scandium and yttrium dialkyl complexes, unexpected reactivity of the yttrium complex with $[\text{CPh}_3][\text{B}(\text{C}_6\text{F}_5)_4]$, and intramolecular hydroamination catalysis.

Results and Discussion

The $\text{H}[\text{All}_2]$ pro-ligand was synthesized via Pd-catalysed imination of 4,5-dibromo-2,7,9,9-tetramethylacridan with two equivalents of 1,3-diisopropylimidazol-2-imine (Scheme 1). Imination reactions utilizing $\text{Ph}_2\text{C}=\text{NH}$ are commonplace, but reactions with other imine substrates have seldom been reported.⁴⁶ In this work, a 4th generation Ruphos catalyst,⁵² combined with high temperature and an extended reaction time was required to access $\text{H}[\text{All}_2]$ in reasonable yield (59%). The room temperature ^1H NMR and ^{13}C NMR spectra of $\text{H}[\text{All}_2]$ are consistent with the expected structure, with four equivalent isopropyl groups due to the accessibility of the zwitterionic resonance form.



Scheme 1. Synthesis of the $\text{H}[\text{All}_2]$ pro-ligand and $[(\text{All}_2)\text{M}(\text{CH}_2\text{SiMe}_3)_2]$ ($\text{M} = \text{Y}$ (1) and Sc (2)) ($\text{Im} = 1,3\text{-diisopropylimidazol-2-ylidene}$).

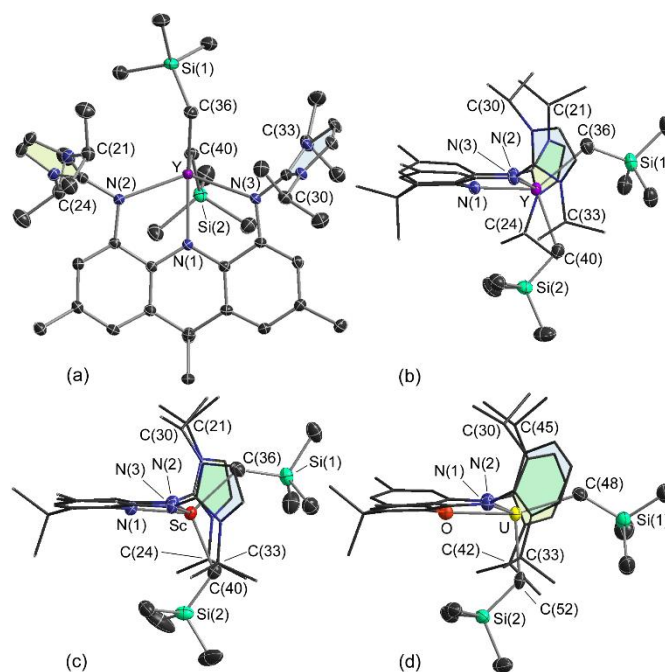


Figure 2. (a-b) Top and side views of the X-ray crystal structure $[(\text{All}_2)\text{Y}(\text{CH}_2\text{SiMe}_3)_2]$ (1). (c) Side view of the X-ray crystal structure of $[(\text{All}_2)\text{Sc}(\text{CH}_2\text{SiMe}_3)_2] \cdot 1.25\text{toluene}$ (2). (d) Side view of the X-ray crystal structure of previously reported $[(\text{XA}_2)\text{U}(\text{CH}_2\text{SiMe}_3)_2] \cdot 2\text{hexane}$.⁸ For (c) and (d), only one of two independent molecules in the unit cell is shown (for 2, the SiMe_3 group attached to C(40A) is disordered over two positions). Ellipsoids are set to 50% (a), 70% (b-c) and 35% (d) probability. For clarity, hydrogen atoms and lattice solvent have been omitted, and in (d), CMe_3 methyl groups are omitted. Flanking imidazole or phenyl rings are shaded in blue or yellow-green (darker green where overlapping). Bond distances (Å) and angles (deg) for 1: Y–C(36) 2.482(2), Y–C(40) 2.434(2), Y–N(1) 2.288(2), Y–N(2) 2.421(2), Y–N(3) 2.394(2), Y–C(36)–Si(1) 116.0(1), Y–C(40)–Si(2) 118.55(9), N(2)–Y–N(3) 133.09(5), N(1)–Y–C(36) 138.82(6), N(1)–Y–C(40) 110.46(6), C(36)–Y–C(40) 110.48(7). Bond distances (Å) and angles (deg) for 2: Sc(1)–C(36) 2.292(2), Sc(1A)–C(36A) 2.295(2), Sc(1)–C(40) 2.267(2), Sc(1A)–C(40A) 2.261(2), Sc(1)–N(1) 2.131(2), Sc(1A)–N(1A) 2.128(2), Sc(1)–N(2) 2.256(2), Sc(1A)–N(2A) 2.255(2), Sc(1)–N(3) 2.251(2), Sc(1A)–N(3A) 2.240(2), Sc(1)–C(36)–Si(1) 126.0(1), Sc(1A)–C(36A)–Si(1A) 124.7(1), Sc(1)–C(40)–Si(2) 121.4(1), Sc(1A)–C(40A)–Si(2A) 121.3(1), N(2)–Sc(1)–N(3) 142.47(5), N(2A)–Sc(1A)–N(3A) 139.34(6), N(1)–Sc(1)–C(36) 132.82(7), N(1A)–Sc(1A)–C(36A) 138.10(8), N(1)–Sc(1)–C(40) 116.30(7), N(1A)–Sc(1A)–C(40A) 113.74(8), C(36)–Sc(1)–C(40) 110.80(8), C(36A)–Sc(1A)–C(40A) 107.9(1).

Reaction of $H[AlI_2]$ with one equivalent of $[M(CH_2SiMe_3)_3(THF)_2]$ ($M = Y, Sc$) yielded the base-free neutral dialkyl complexes $[(AlI_2)M(CH_2SiMe_3)_2]$ ($M = Y$ (**1**) and Sc (**2**)) in high yield (>90%) as analytically pure beige solids (Scheme 2). Both **1** and **2** are stable at room temperature, with apparent C_{2v} symmetry between 20 and -60 °C in solution, due to a fluxional process involving exchange of the alkyl groups between coordination sites above/below the plane of the ligand, and in the plane of the ligand. The MCH_2 1H and ^{13}C NMR signals were located at -0.81 and 28.32 ppm ($^1J_{13C,89Y}$ 36 Hz; $^2J_{1H,89Y}$ 2 Hz) for **1** and -0.50 and 30.97 ppm for **2**. The $^1J_{C,H}$ coupling constant for the MCH_2 signal in **1** and **2** is 101–102 Hz.

X-ray quality crystals of **1** (a–b in Figure 2) and **2**·1.25 toluene (c in Figure 2) were grown from toluene at -28 °C; **2** contains two independent but qualitatively isostructural molecules in the unit cell. In both **1** and **2**, the AlI_2 ligand is κ^3 -coordinated with an angle of 28.6° (for **1**) or 12.0° and 19.3° (for **2**) between the two aryl rings of the acridanide backbone. The metal is 5-coordinate, with one alkyl group {C(36)} located between the flanking imidazole rings, whereas the other {C(40)} is located below the plane of the ligand backbone, flanked by isopropyl groups {the C(21)–C(30) and C(24)–C(33) distances are 6.55 and 8.21 Å in **1**, and 6.51 and 7.59 Å or 6.14 and 7.70 Å in **2**}.

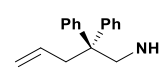
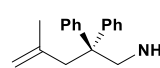
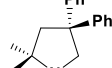
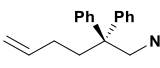
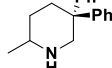
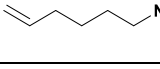
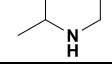
In compound **1**, the Y–C(36) and Y–C(40) distances are 2.482(2) and 2.434(2) Å, respectively, which lie at the upper end of the range for monometallic yttrium trimethylsilylmethyl complexes (which are commonly 2.36 to 2.47 Å).⁵³ The Y–N(1) distance to the central amido donor is 2.288(2) Å, whereas the Y–N(2) and Y–N(3) bond lengths are 2.421(2) and 2.394(2) Å, consistent with weaker coordination of the neutral imidazol-2-imine donors. The Y–N_{imine} distances in **1** are shorter than the Y–N_{imine} distances of 2.475(5) and 2.494(4) Å to the intact Alm_2 ligand in $[Y(Alm_2)(Alm_2')]$ (Alm_2' is a cyclometallated Alm_2 ligand),³⁴ but longer than the Y–N_{imine} distances of 2.381(2) and 2.358(2) Å in Tamm's $\{[2,6-C_5H_3N(CH_2N=Im)_2]YCl_3\}$ ($Im = 1,3$ -di-*tert*-butylimidazol-2-ylidene).³⁹ All M–C and M–N bonds in **2** are shorter than those in **1** by 0.14–0.19 Å, primarily reflecting the difference in the ionic radii of Sc(III) and Y(III) (0.745 vs 0.90 Å).⁵⁴ The M–C–Si angles are $116.0(1)$ and $118.55(9)^\circ$ in **1**, and $121.4(1)$ – $126.0(1)^\circ$ in **2**.

The N(2)–C_{imine} and N(3)–C_{imine} bond distances in **1** and **2** range from 1.357(2) to 1.368(3) Å, which is significantly longer than in free imidazol-2-imines. For example, the N=C distances in the free imines in $Im=N\{C_6H_4(OMe)-p\}$ ($Im = 1,3$ -diisopropyl-4,5-dimethylimidazol-2-ylidene)⁵⁵ and $\{[\kappa^2-2,6-C_5H_3N(CH_2N=Im)_2]FeCl_2\}$ ($Im = 1,3$ -di-*tert*-butylimidazol-2-ylidene)⁵⁶ are 1.308(2) and 1.294(3) Å, respectively. Furthermore, the endocyclic N–C_{imine} distances in **1** and **2** (1.357(2)–1.364(2) Å) are comparable to the exocyclic N(2)–C_{imine} and N(3)–C_{imine} distances. These features, and the roughly perpendicular orientation of the imidazole rings relative to the adjacent aryl ring of the acridanide backbone (the interplanar angles are 63.5° and 82.5° in **1**, and 75.6 – 87.3° in **2**), are indicative of a substantial contribution from the zwitterionic resonance structure with negative charges on N(2) and N(3).

The uranium(IV) complex $[(XA_2)U(CH_2SiMe_3)_2]$ (d in Figure 2)⁸ allows for a comparison of the steric profiles of the

monoanionic AlI_2 and dianionic XA_2 ligands, given that the ionic radii of yttrium(III) and uranium(IV) are very similar (0.90 vs 0.89 Å). Compound **1** and $[(XA_2)U(CH_2SiMe_3)_2]$ (which contains two independent but qualitatively isostructural molecules in the unit cell) are structurally similar, and the C–N–C angles around the flanking nitrogen donors are nearly identical (114 – 121°). However, the N–N distance between the flanking nitrogen donors in the uranium complex is substantially shorter (ave. 4.00 for the uranium XA_2 complex vs 4.42 Å for the yttrium AlI_2 complex) due to shorter M–N_{amido} vs M–N_{imine} distances. This contributes to shorter C–C distances between flanking isopropyl methine carbon atoms in the uranium complex {C(30)–C(45) = 4.60–4.85 Å; C(33)–C(42) = 7.65–7.70 Å}, indicating that the anionic 2,6-diisopropylphenylamido groups in XA_2 exert a greater steric influence than the neutral 1,3-diisopropylimidazol-2-imine donors in AlI_2 . A knock-on effect of the short C(30)–C(45) distance (combined with an average M–C distance that is 0.07 Å shorter) in the uranium complex is that the alkyl ligands move away from the more sterically hindered side of the ligand (where C(30) and C(45) are located), resulting in O–U–C(52) angles of $94.8(2)$ and $95.0(2)^\circ$, and C(48)–U–C(52) angles of $103.2(2)$ and $105.0(2)^\circ$, which are more acute than the corresponding N(1)–Y–C(40) and C(36)–Y–C(40) angles in **1** { $110.46(6)$ and $110.48(7)^\circ$ }.

Table 1. Intramolecular hydroamination catalyzed by $1/[CPh_3][B(C_6F_5)_4]$ {2 mol % (Entry 1) or 5 mol % (Entries 2–4)}. Reactions were conducted in 0.8 mL C_6D_5Br , at 25 °C unless otherwise indicated.

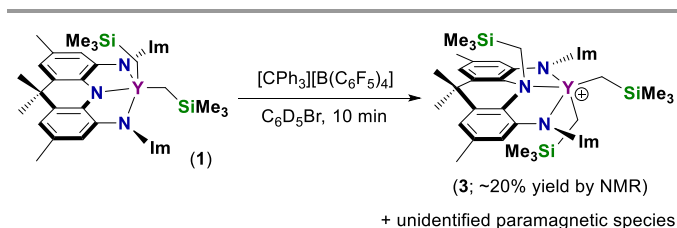
	Substrate	Product	Time (h)	% ^a	N_T (h^{-1})
1			≤ 0.13	≥ 99	≥ 385
2			1	> 99	20
3			1.1	> 99	18.5
4 ^b			36	0	0

^a Percentage conversion to product relative to an internal standard (ferrocene), determined by 1H NMR spectroscopy. ^b 25–80 °C.

Reaction of **1** with one equiv. of $[CPh_3][B(C_6F_5)_4]$ in C_6D_5Br afforded a highly active catalyst for intramolecular alkene hydroamination.^{57–61} For example, the cyclization of 1-amino-2,2-diphenyl-4-pentene using 2 mol% of $1/[CPh_3][B(C_6F_5)_4]$ (Entry 1 in Table 1) was complete after 8 minutes at room temperature, corresponding to a turnover number of $\geq 385 h^{-1}$. Additionally, $1/[CPh_3][B(C_6F_5)_4]$ (5 mol%; Entries 2–3) cyclized 1-amino-2,2-diphenyl-4-methyl-4-pentene and 1-amino-2,2-diphenyl-5-hexene (>99% completion) in just 1.1–1.5 hours at room temperature. These substrates are more challenging than 1-amino-2,2-diphenyl-4-pentene due to increased alkene steric hindrance and less favourable six- versus five-membered ring

formation, respectively, and catalysts capable of cyclizing these substrates at room temperature are uncommon. These reactions (with 2 or 3.75 mol% catalyst loading) were found to be zero order with respect to substrate concentration (Figures S51-52), suggestive of rate-determining 1,2-insertion.⁶² Attempts to cyclize 1-amino-5-hexene proved unsuccessful between 24 and 80 °C (Entry 4), which can be attributed to the absence of cyclization-promoting phenyl groups (Thorpe-Ingold effect),⁶³ and strong coordination of the sterically unencumbered substrate to yttrium. In contrast to the high intramolecular hydroamination activity of **1**/[CPh₃][B(C₆F₅)₄], a 5 mol% catalyst loading of neutral **1** required 5.1 hours to complete the room temperature cyclization of 1-amino-2,2-diphenyl-4-pentene. This reaction was also zero order with respect to substrate concentration (Figure S50). Hydroamination catalysts prepared by reaction of a polyalkyl rare earth complex with [CPh₃][B(C₆F₅)₄] have only occasionally been investigated, but have been reported to give rise to either significantly lower or higher catalytic activity relative to the neutral polyalkyl precursor.^{62,64-67}

The aforementioned reaction of **1** with [CPh₃][B(C₆F₅)₄]⁺ (Scheme 2) in C₆D₅Br afforded a deep purple solution, with a small amount of colourless precipitate, and ¹H NMR spectroscopy in the presence of an internal standard (naphthalene) showed the formation of one major diamagnetic complex (*vide infra*)[†] in ~20 % yield, accompanied by HCPH₃ (by integration, ~2 equiv. relative to the diamagnetic complex). Other products are presumed to be insoluble or paramagnetic (potentially giving rise to the purple colour of the solution), and indeed, room temperature EPR spectroscopy revealed a nonet at *g* = 2.0098 (Figure S43). The observed *g*-value is consistent with an organic-based radical, and the splitting pattern is adequately modelled by hyperfine coupling to one ¹⁴N and six ¹H atoms (Figure S43; *a*(¹⁴N) = 13.1 MHz; *a*(¹H) = 10.9 (2H), 12.8 (2H), and 15.5 (2H) MHz), although other coupling schemes are possible.⁵



Scheme 2. Reaction of [(All₂Y(CH₂SiMe₃)₂)] (**1**) with [CPh₃][B(C₆F₅)₄] to afford [(All₂-CH₂SiMe₃)Y(CH₂SiMe₃)₂][B(C₆F₅)₄] (**3**) in ~20% spectroscopic yield. This reaction also generated HCPH₃ (~ 2 equiv. relative to **3**) and an unidentified paramagnetic product.

Formation of the paramagnetic product likely involves initial oxidation of **1** at the ligand backbone,[†] given that the zwitterionic form of the ligand contains a phenylene ring with two adjacent anionic nitrogen donors, similar to a redox-non-innocent, dianionic *ortho*-phenylenediamido ligand {*o*-C₆H₄(NR)₂}.⁶⁸⁻⁷⁰ Indeed, cyclic voltammetry of **1** in 1,2-difluorobenzene / [NBu₄][B(C₆F₅)₄] (Figures S45-46) showed an oxidation wave (partially reversible at a scan rate of 200 mV s⁻¹; qualitatively reversible at 2.00 V s⁻¹) with an *E*_{1/2} value of –

0.90 V versus [FeCp₂]^{0/+}, indicating that **1** can readily be oxidized by CPh₃⁺, which has a redox potential of –0.24 V versus [FeCp₂]^{0/+} in CH₂Cl₂ / [NBu₄][BF₄].⁷¹ Redox non-innocent behaviour was also recently reported for a related 4,5-bis(amido)acridanide ligand coordinated to tantalum.⁷² However, it is interesting to note that in the reaction of **1** with CPh₃⁺, triphenylmethane is the major organic byproduct, rather than Gomberg's dimer {(CPh₃)₂}, which was not detected, suggesting additional reactivity involving hydrogen atom abstraction by the ·CPh₃ byproduct.

¹H NMR spectra of the reaction of **1** with [CPh₃][B(C₆F₅)₄] revealed that the diamagnetic product contains one All₂ ligand environment with side-to-side symmetry (giving rise to one C^{2,7}Me, CH^{1,8} and CH^{3,6} environment), but top-bottom asymmetry (giving rise to two CMe₂, two CHMe₂, and four CHMe₂ resonances). This symmetry is consistent with the initially expected [(All₂)Y(CH₂SiMe₃)][B(C₆F₅)₄] cation. However, three CH₂SiMe₃ groups are observed in the ¹H NMR spectrum, none of which have chemical shifts matching the typical byproducts formed in reactions of CPh₃⁺ with trimethylsilylmethyl complexes.^{11,73} Furthermore, all three CH₂SiMe₃ groups show HMBC and/or NOESY peaks indicating that they are part of the same complex (Figure 3). Two of the CH₂SiMe₃ groups gave rise to low-frequency CH₂ signals (–0.24 and –0.32 ppm) in the ¹H NMR spectrum, consistent with yttrium alkyl groups. By contrast, one CH₂SiMe₃ group afforded a CH₂ signal at 3.37 ppm, indicative of attachment to an electronegative atom, and this CH₂ signal also shows an HMBC correlation to the C^{11,12} quaternary carbon atoms of the ligand backbone (see numbering in Scheme 1). These data indicate that this third CH₂SiMe₃ group is attached to the central nitrogen atom of the ligand backbone to afford [(All₂-CH₂SiMe₃)Y(CH₂SiMe₃)₂][B(C₆F₅)₄] (**3**), where All₂-CH₂SiMe₃ is a neutral tridentate ligand with a central amine donor flanked by imidazolin-2-imine groups (Scheme 2). For comparison, the ¹H NMR chemical shift, in CDCl₃, for the NCH₂ group in Ph₂NCH₂SiMe₃ is 3.34 ppm (and the NCH₂ chemical shift in the ¹³C NMR spectrum is 43.7 ppm; cf. 39.8 ppm in **3**).⁷⁴

Multiple attempts to obtain single crystals of **3** were unsuccessful, but NOESY correlations (Figure 3) between the three CH₂SiMe₃ groups and the neighboring CHMe₂ and ligand backbone CMe₂ groups further support the identity of compound **3**. The ¹¹B and ¹³C NMR chemical shifts are consistent with an intact B(C₆F₅)₄⁻ anion,⁷⁵ although in the ¹⁹F NMR spectrum, the *para* and *meta* signals are extremely broad (between 25 and –25 °C), likely due to interactions with the unidentified (and presumably cationic) paramagnetic species.

The reaction pathway responsible for the formation of **3** has not been determined, but is likely to involve initial ligand backbone oxidation by CPh₃⁺ with subsequent C–N coupling, potentially occurring via a radical mechanism.⁷⁶⁻⁸¹ Oxidation of metal alkyl complexes by CPh₃⁺ has various literature precedent. For example, [Cp₂WMe₂] reacted with CPh₃⁺ to afford [Cp₂WH(C₂H₄)]⁺ and HCPH₃ via oxidation of the tungsten complex by CPh₃⁺, followed by hydrogen atom abstraction by the trityl radical to generate [Cp₂W(=CH₂)Me]⁺, and ensuing

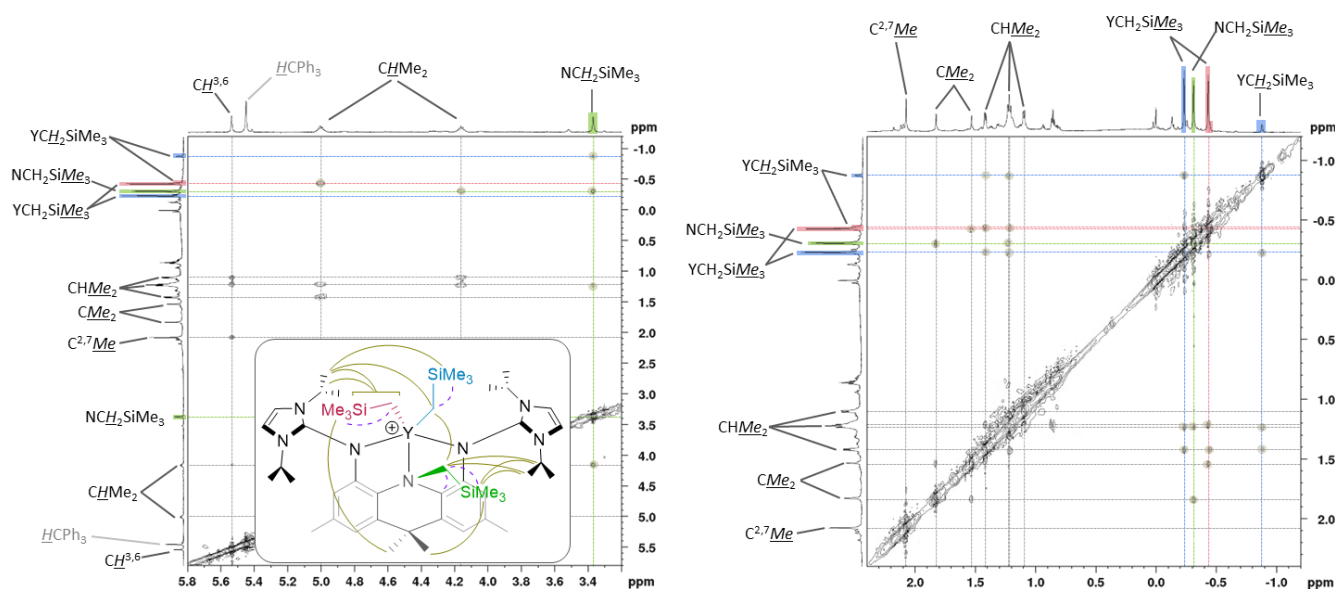


Figure 3. Selected regions of the 2D ^1H - ^1H NOESY NMR spectrum for in-situ-generated $[(\text{All}_2\text{-CH}_2\text{SiMe}_3)\text{Y}(\text{CH}_2\text{SiMe}_3)_2][\text{B}(\text{C}_6\text{F}_5)_4]$ (**3**). Crosspeaks involving the CH_2SiMe_3 groups are highlighted. On the axes, $\text{YCH}_2\text{SiMe}_3$ peaks are indicated in blue and red, and the $\text{NCH}_2\text{SiMe}_3$ peaks are highlighted in green. The chemdraw structure (with CH_2SiMe_3 groups colour coded to match the peaks on the axes of the NOESY spectra) shows NOESY correlations (those involving the CH_2SiMe_3 groups) as curved solid lines and indicates key HMBC correlations as purple dashed lines.

1,1-insertion and β -hydride elimination.⁸² Similarly, $[\text{Cp}^*\text{IrMe}_2(\text{PMe}_3)]$ reacted with CPh_3^+ to afford $[\text{Cp}^*\text{IrH}(\text{C}_2\text{H}_4)(\text{PMe}_3)]^+$ and HCPH_3 (accompanied by a small amount of the tetramethylfulvene complex $[(\text{C}_5\text{Me}_4\text{CH}_2)\text{IrMe}_2(\text{PMe}_3)]^+$), and this reactivity was proposed to involve initial electron transfer followed by hydrogen atom abstraction.⁸³ The reaction of $[(\text{Im}=\text{N})_2\text{TiMe}_2]$ ($\text{Im} = 1,3\text{-di-}t\text{-butylimidazol-2-ylidene}$) with CPh_3^+ also failed to generate the expected titanium(IV) alkyl cation, instead yielding unidentified paramagnetic species.⁸⁴ Additionally, metal hydride complexes have been shown to react with CPh_3^+ via initial electron transfer. For example, the reaction of $[\text{CpMoH}(\text{CO})(\text{dppe})]$ ($\text{dppe} = 1,2\text{-bis}(\text{diphenylphosphino})\text{ethane}$) with CPh_3^+ in MeCN generated $[\text{CpMo}(\text{CO})(\text{dppe})(\text{NCMe})]^+$, accompanied by H_2 and half an equivalent of Gomberg's dimer. This reaction was proposed to involve one-electron oxidation, proton transfer from $[\text{CpMoH}(\text{CO})(\text{dppe})]^+$ to remaining $[\text{CpMoH}(\text{CO})(\text{dppe})]$, loss of H_2 from $[\text{CpMoH}_2(\text{CO})(\text{dppe})]^+$ followed by MeCN coordination, and oxidation of $[\text{CpMo}(\text{CO})(\text{dppe})]$ by CPh_3^+ , with accompanying MeCN coordination.⁸⁵ Similarly, the room temperature reaction of $[\text{CpRuH}(\text{PPh}_3)_2]$ with CTol_3^+ ($\text{Tol} = p\text{-tolyl}$) afforded a mixture of $[(\text{C}_5\text{H}_4\text{CTol}_3)\text{RuH}_2(\text{PPh}_3)_2]^+$, $[\text{CpRuH}_2(\text{PPh}_3)_2]^+$, $[\text{CpRu}(\text{PPh}_3)_2(\text{NCMe})]^+$, $[\text{CpRu}(\text{PPh}_3)_2(\text{NCMe})]^+$, and a minor unidentified product; this reactivity was again proposed to involve initial electron

transfer.⁸⁶ It is also notable that even for typical reactions of CPh_3^+ with $[\text{L}_x\text{M}(\text{CH}_2\text{SiMe}_3)_2]$ (to generate the expected metal alkyl cation), the organic reaction byproducts are usually more complex than might be expected, consisting of two products containing a CH_2SiMe_3 group, and a small amount (e.g. 10%) of HCPH_3 .^{11,73}

Summary and Conclusions

A rigid new NNN-donor pincer ligand employing an anionic acridanide backbone with flanking neutral imidazolin-2-imine donors was synthesized (as the protio ligand) and reactions with $[\text{M}(\text{CH}_2\text{SiMe}_3)_3(\text{THF})_2]$ afforded neutral base-free dialkyl complexes of yttrium and scandium, $[(\text{All}_2)\text{M}(\text{CH}_2\text{SiMe}_3)_2]$ $\{\text{M} = \text{Y}$ (**1**) and Sc (**2**) $\}$. The reactivity of $\text{H}[\text{All}_2]$ differs significantly from that of previously reported 4,5-bis{(diphenylmethylene)-amino}-2,7,9,9-tetramethylacridan ($\text{H}[\text{Alm}_2]$), which was insufficiently bulky to prevent installation of 2 equivalents of the ligand on yttrium, and rapid cyclometallation.³⁴ Complexes **1** and **2** are stable at room temperature, and the solid-state structures highlight the extent to which the monoanionic All_2 ligand possesses a similar, but slightly tempered, steric profile to the previously reported XA_2 dianion.

Reaction of **1** with $[\text{CPh}_3][\text{B}(\text{C}_6\text{F}_5)_4]$ unexpectedly generated a dialkyl yttrium cation, $[(\text{All}_2\text{-CH}_2\text{SiMe}_3)\text{Y}(\text{CH}_2\text{SiMe}_3)_2][\text{B}(\text{C}_6\text{F}_5)_4]$

(**3**), where $\text{AlI}_2\text{-CH}_2\text{SiMe}_3$ is a neutral tridentate ligand with a central amine donor flanked by imidazolin-2-imine groups. Compound **3** was formed in ~20% spectroscopic yield, accompanied by HCPH_3 (~2 equiv. relative to **3**), a small amount of precipitate, and an unidentified paramagnetic product. The reaction to form **3** involves coupling of an alkyl and an amido group at yttrium, and is suggested to involve initial AlI_2 ligand backbone oxidation rather than alkyl anion abstraction, given that the zwitterionic form of the ligand contains a phenylene ring with two adjacent anionic nitrogen donors, similar to a redox-non-innocent, dianionic *ortho*-phenylenediamido ligand. The formation of **3** underscores the potential for unexpected outcomes in reactions of alkyl complexes with CPh_3^+ , especially when ligand-based redox reactivity can occur.

Despite the complex reactivity of **1** with $[\text{CPh}_3][\text{B}(\text{C}_6\text{F}_5)_4]$, this combination afforded a highly active catalyst for intramolecular alkene hydroamination, whereas unactivated **1** was poorly active. For both **1** and $1/[\text{CPh}_3][\text{B}(\text{C}_6\text{F}_5)_4]$, a zero order dependence on substrate concentration suggests that the rate determining step is 1,2-insertion, as opposed to protonation by substrate to release the cyclized product.

Experimental Section

General Details: An argon-filled M-Braun UNILab glovebox equipped with a -28°C freezer was employed for the manipulation and storage of all air sensitive compounds, and reactions were performed on a double manifold high vacuum line (with all glass-glass connections, rather than connections via hose tubing) using standard techniques. The vacuum line operated at <5 mTorr, and the argon stream for the vacuum line was purified using an Oxisorb-W scrubber from Matheson Gas Products. A Fisher Scientific Ultrasonic FS-30 bath was used to sonicate reaction mixtures where indicated. Hexanes and pentane were initially dried and distilled at atmospheric pressure from $\text{Na}/\text{Ph}_2\text{CO}$. Toluene was initially dried and distilled at atmospheric pressure from Na . Unless otherwise indicated, all proteo solvents were stored over an appropriate drying agent [pentane, hexanes: $\text{Na}/\text{Ph}_2\text{CO}/\text{tetraglyme}$; toluene: $\text{Na}/\text{Ph}_2\text{CO}$; 1,4-dioxane: 4\AA molecular sieves] and vacuum distilled into reaction flasks or storage flasks for use within a glovebox. Deuterated solvents were purchased from Cambridge Isotope Laboratories; C_6D_6 was dried over $\text{Na}/\text{Ph}_2\text{CO}/\text{tetraglyme}$, and $\text{C}_6\text{D}_5\text{Br}$ was dried over 4\AA molecular sieves.

$[\text{Y}(\text{CH}_2\text{SiMe}_3)_3(\text{THF})_2]_2$,⁸⁷ $[\text{Sc}(\text{CH}_2\text{SiMe}_3)_3(\text{THF})_2]_2$,⁸⁸ $[\text{FeCp}_2][\text{B}(\text{C}_6\text{F}_5)_4]$,⁸⁹ and 1,3-diisopropylimidazol-2-imine⁹⁰ were synthesized using literature procedures. 4,5-dibromo-2,7,9,9-tetramethylacridan was also synthesized via the literature procedure,³⁴ with purification by column chromatography using silica/hexanes, followed by heating at 70°C to remove unknown volatile impurities, and then sublimation at 110°C . $\text{LiCH}_2\text{SiMe}_3$ (1.0M in pentane), 1,3-diisopropylimidazolium chloride, anhydrous YCl_3 , anhydrous ScCl_3 , NaO^tBu , RuPhos ($\text{PCy}_2\{o\text{-C}_6\text{H}_4(\text{C}_6\text{H}_3\{\text{O}^i\text{Pr}\}_2\text{-2,6})\}$), and "RuPhos Pd G4" ($[(\text{RuPhos})\text{Pd}(\text{C}_6\text{H}_4\{o\text{-C}_6\text{H}_4(o\text{-NHMe})\})\text{(OMs)}]$; OMs = OSO_2Me) were purchased from Sigma Aldrich. $\text{YCl}_3(\text{THF})_{3,5}$ and $\text{ScCl}_3(\text{THF})_3$

were obtained by refluxing anhydrous MCl_3 ($\text{M} = \text{Y}, \text{Sc}$) in dry THF for 24 hours, followed by removal of solvent in vacuo. $[\text{CPh}_3][\text{B}(\text{C}_6\text{F}_5)_4]$ was purchased from Alfa Aesar or Strem. Argon (99.999%) was purchased from Praxair. 1-Amino-2,2-diphenylpent-4-ene, 1-amino-2,2-diphenyl-4-methylpent-4-ene and 1-amino-2,2-diphenylhex-5-ene were synthesized using literature procedures^{14,91} and dried over 4\AA molecular sieves. 1-Amino-5-hexene was purchased from GFS Chemicals, dried over 4\AA molecular sieves and degassed in vacuo.

Combustion elemental analyses were performed by Midwest Microlab, LLC, Indianapolis, Indiana. Cyclic voltammetry was performed within a glovebox using a Pine Research WaveNow Wireless potentiostat/galvanostat (using AfterMath software), a platinum wire counter electrode, a silver wire pseudo-reference electrode, and a platinum disc working electrode (1.6 mm diameter, Bioanalytical Systems). Solutions were 1×10^{-3} M in the test compound and 0.1 M in $[\text{N}^t\text{Bu}_4][\text{B}(\text{C}_6\text{F}_5)_4]$ as the base electrolyte. $[\text{FeCp}^*_2]$ was added at the end of the experiment, as an internal calibrant, and all quoted potentials are relative to $[\text{FeCp}_2]^{0/+}$ (converted using a measured $E_{1/2}$ value of -0.60 V for $[\text{FeCp}^*_2]^{0/+}$ versus $[\text{FeCp}_2]^{0/+}$ in 1,2-difluorobenzene / $[\text{N}^t\text{Bu}_4][\text{B}(\text{C}_6\text{F}_5)_4]$). NMR spectroscopy (^1H , $^{13}\text{C}\{^1\text{H}\}$, DEPT-Q, COSY, HSQC, HMBC, ^{19}F , ^{11}B) was performed on a Bruker AV-600 Spectrometer and a Bruker AV-500 Spectrometer. Low-T NMR was conducted exclusively on the AV-500 Spectrometer. All ^1H NMR and ^{13}C NMR spectra are referenced relative to SiMe_4 using the resonance of the deuterated solvent (^{13}C NMR) or protio impurity in the deuterated solvent (^1H NMR); in ^1H NMR, 7.16 ppm for C_6D_6 , and 7.30, 7.02 and 6.94 ppm for $\text{C}_6\text{D}_5\text{Br}$; in ^{13}C NMR, 128.06 ppm for C_6D_6 , and 130.90, 129.41, 126.24 and 122.17 ppm for $\text{C}_6\text{D}_5\text{Br}$. EPR spectroscopy was performed on a Bruker EMXmicro X-band EPR spectrometer, and spectra were modelled using the cwEPR app (version 3.4.10)⁹² within EasySpin (version 5.2.35)⁹³ running in Matlab. X-ray crystallographic analyses were performed on suitable crystals coated in Paratone oil and mounted on a SMART APEX II diffractometer with a 3 kW Sealed tube Mo generator in the McMaster Analytical X-ray (MAX) Diffraction Facility. In all cases, non-hydrogen atoms were refined anisotropically and H atoms were generated in ideal positions and updated with each cycle of refinement.

4,5-(1,3-diisopropylimidazol-2-imino)-2,7,9,9-tetramethylacridan (H[AlI₂]): Under argon, a mixture of $[(\text{RuPhos})\text{Pd}(\text{C}_6\text{H}_4\{o\text{-C}_6\text{H}_4(o\text{-NHMe})\})\text{(OMs)}]$ ("RuPhos Pd G4"; 214 mg, 0.252 mmol), RuPhos (117.9 mg, 0.252 mmol) and sodium *tert*-butoxide (0.584 g, 6.07 mmol) was dissolved in approximately 10 mL of 1,4-dioxane and stirred for 5 minutes in a 100 mL sealed flask. This was followed by the addition of 1,3-diisopropylimidazol-2-imine (0.888 g, 5.31 mmol) and 4,5-dibromo-2,7,9,9-tetramethylacridan (1.00 g, 1.761 mmol) in approximately 30 mL of 1,4-dioxane. The sealed reaction flask was heated at 100°C in an oil bath for 36 h yielding a dark brown or dark purple solution. In a glovebox, the reaction solution was centrifuged, and volatiles were removed from the mother liquors in vacuo to afford a dark brown oil. The product was then exposed to air, and extracted using approximately 30 mL

of CH₂Cl₂. This organic layer was washed with a total of 60 mL of water, the resulting aqueous layer was extracted with 30 mL of CH₂Cl₂, and the organic layers were combined. The organic layer was dried over MgSO₄ and gravity filtered. Volatiles were removed from the filtrate under reduced pressure to afford a sticky dark brown solid. This solid was dissolved in approximately 60 mL of hot hexanes and was passed through a pad of Celite, yielding a dark orange filtrate. The filtrate was concentrated to 20 mL and was allowed to re-crystallize at -10 °C overnight. The resulting brown-orange powder was dried for 12 h at 80 °C under reduced pressure to yield 846 mg of H[AlI₂] (59 % yield). Note: this synthesis seemed to be very sensitive to the presence of impurities in the 4,5-dibromo-2,7,9,9-tetramethylacridan, and in some cases, the addition of more catalyst was required for the reaction to proceed. ¹H NMR (C₆D₆, 600 MHz, 298K): δ 8.39 (s, 1H, NH), 6.98 (s, 2H, CH^{1,8}), 6.72 (s, 2H, CH^{3,6}), 5.90 (s, 4H, N-CH), 4.49 (sept, ³J_{H,H} 6.0 Hz, 4H, CHMe₂), 2.39 (s, 6H, Ar-Me), 1.82 (s, 6H, CMe₂), 0.92 (d, ³J_{H,H} 6.0 Hz, 24H, CHMe₂). ¹³C{¹H} NMR (C₆D₆, 151 MHz, 298K): δ 146.45 (s, NCN), 137.27 (s, C^{4,5}), 131.64 (s, C^{11,12}), 128.94 (s, C^{10,13}), 127.28 (s, C^{2,7}), 116.83 (s, CH^{3,6}), 116.24 (s, CH^{1,8}), 108.61 (s, N-CH), 45.69 (s, CHMe₂), 37.33 (s, C⁹), 29.96 (s, CMe₂), 21.83 (s, Ar-Me), 21.42 (s, CHMe₂). C₃₅H₄₉N₇ (567.83 g mol⁻¹): calcd. C 74.03, H 8.70, N 17.27 %; found. C 73.75, H 8.85, N 17.05 %.

[(All₂)Y(CH₂SiMe₃)₂] (1): A solution of H[All₂] (484 mg, 0.852 mmol) in 20 mL of toluene was added dropwise to a solution of [Y(CH₂SiMe₃)₃(thf)₂] (422 mg, 0.852 mmol) in toluene (15 mL) at room temperature. The reaction was stirred for 1 hour and then the solvent was removed in vacuo to afford an orange-brown oil. 30 mL of hexanes was added to the oil and the mixture was sonicated to obtain a beige solid. Solvent was removed in vacuo and the solid was washed with hexanes (3 x ~ 5 mL). The solid was dried under vacuum for 4 hours, yielding **1** as a highly air-sensitive pale beige solid (658 mg, 93 % yield). X-ray quality crystals of **1** were grown by cooling a concentrated toluene solution to -28 °C. ¹H NMR (C₆D₆, 600 MHz, 298K): δ 6.92 (s, 2H, CH^{1,8}), 6.06 (s, 4H, N-CH), 5.56 (s, 2H, CH^{3,6}), 4.88 (sept, ³J_{H,H} 7 Hz, 4H, CHMe₂), 2.27 (s, 6H, Ar-Me), 1.96 (s, 6H, CMe₂), 1.19 (d, ³J_{H,H} 7 Hz, 12H, CHMe₂), 0.99 (d, ³J_{H,H} 7 Hz, 12H, CHMe₂), 0.19 (s, 18H, CH₂SiMe₃), -0.81 (d, ²J_{H,Y} 2 Hz, 4H, CH₂SiMe₃). ¹³C{¹H} NMR (C₆D₆, 151 MHz, 298K): δ 152.21 (s, NCN), 144.31 (s, C^{4,5}), 139.33 (s, C^{2,7}), 127.77 (s, C^{11,12}), 123.48 (s, C^{10,13}), 118.04 (s, CH^{1,8}), 112.45 (s, N-CH), 111.71 (s, CH^{3,6}), 47.62 (s, CHMe₂), 37.11 (s, C⁹), 34.46 (s, CMe₂), 28.32 (d, ¹J_{C,Y} 36 Hz, CH₂SiMe₃), 23.06 (s, CHMe₂), 22.29 (s, CHMe₂), 21.94 (s, Ar-Me), 4.62 (s, CH₂SiMe₃). C₄₃H₇₀N₇Si₂Y (830.16 g mol⁻¹): calcd. C 62.21, H 8.50, N 11.81 %; found. C 61.68, H 8.44, N 11.25 %.

[(All₂)Sc(CH₂SiMe₃)₂] (2): A solution of H[All₂] (100 mg, 0.176 mmol) in 10 mL of toluene was added dropwise to a solution of [Sc(CH₂SiMe₃)₃(thf)₂] (87.3 mg, 0.193 mmol) in toluene (10 mL) at room temperature. The reaction was stirred for 1 hour and then the solvent was removed in vacuo to afford a brownish oil. 20 mL of hexanes was added to the oil and the mixture was sonicated to obtain a beige solid. Solvent was removed in vacuo and the solid was washed with hexanes (3 x ~ 2 mL). The solid was dried under vacuum for 4 hours yielding **2** as a highly air-

sensitive beige solid (135 mg, 98 % yield). X-ray quality crystals of **2**·1.25 toluene were grown by cooling a concentrated toluene solution to -28 °C. ¹H NMR (C₆D₆, 600 MHz, 298K): δ 6.88 (s, 2H, CH^{1,8}), 6.11 (s, 4H, N-CH), 5.47 (s, 2H, CH^{3,6}), 4.98 (sept, ³J_{H,H} 7 Hz, 4H, CHMe₂), 2.28 (s, 6H, Ar-Me), 1.97 (s, 6H, CMe₂), 1.22 (d, ³J_{H,H} 7 Hz, 12H, CHMe₂), 1.02 (d, ³J_{H,H} 7 Hz, 12H, CHMe₂), 0.13 (s, 18H, CH₂SiMe₃), -0.50 (s, 4H, CH₂SiMe₃). ¹³C{¹H} NMR (C₆D₆, 151 MHz, 298K): δ 153.03 (s, NCN), 145.26 (s, C^{4,5}), 138.23 (s, C^{2,7}), 126.67 (s, C^{11,12}), 123.81 (s, C^{10,13}), 117.18 (s, CH^{1,8}), 112.68 (s, N-CH), 110.22 (s, CH^{3,6}), 47.56 (s, CHMe₂), 36.98 (s, C⁹), 34.35 (s, CMe₂), 30.97 (s, CH₂SiMe₃), 23.55 (s, CHMe₂), 22.13 (s, CHMe₂), 22.13 (s, Ar-Me), 4.31 (s, CH₂SiMe₃). C₄₃H₇₀N₇Si₂Sc (786.19 g mol⁻¹): calcd. C 65.69, H 8.97, N 12.47 %; found. C 65.42, H 8.78, N 11.91 %.

In-situ Synthesis of [(All₂-CH₂SiMe₃)Y(CH₂SiMe₃)₂][B(C₆F₅)₄] (3): 15 mg (0.018 mmol) of [(All₂)Y(CH₂SiMe₃)₂] (**1**) was dissolved in approximately 0.4 mL of C₆D₅Br to afford a light brown solution. To this solution was added [CPh₃][B(C₆F₅)₄] (16.6 mg, 0.018 mmol) in approximately 0.4 mL of C₆D₅Br, rapidly forming a deep purple solution, with some suspended colourless precipitate. The reaction was shown to be complete after 10 minutes by ¹H NMR spectroscopy [this reaction generated **3** in approx. 20% yield (as the only soluble, diamagnetic yttrium-containing product), accompanied by HCPPh₃ (~2 equiv. relative to **3**) and an unidentified paramagnetic product, in addition to the colourless precipitate]. EPR spectra were obtained after dilution of a portion of the reaction mixture. ¹H NMR (C₆D₅Br, 500 MHz, 298K): δ 6.72 (s, 2H, CH^{1,8}), 6.65, 6.63 (s, 2 x 2H, NCH), 5.53 (s, 2H, CH^{3,6}), 5.01 (sept, ³J_{H,H} 7 Hz, 2H, CHMe₂), 4.17 (sept, ³J_{H,H} 7 Hz, 2H, CHMe₂), 3.37 (s, 2H, NCH₂SiMe₃), 2.07 (s, 6H, C^{2,7}Me), 1.82, 1.52 (s, 2 x 3H, CMe₂), 1.42 (d, ³J_{H,H} 7 Hz, 6H, CHMe₂), 1.22 (appt t, ³J_{H,H} 7 Hz, 12H, 2 x CHMe₂), 1.10 (d, ³J_{H,H} 7 Hz, 6H, CHMe₂), -0.24 (s, 9H, YCH₂SiMe₃ A), -0.32 (s, 9H, NCH₂SiMe₃), -0.44 (s, 9H, YCH₂SiMe₃ B), -0.44 (s, 2H, YCH₂SiMe₃ B), -0.88 (s, 2H, YCH₂SiMe₃ A). ¹³C{¹H} NMR (C₆D₅Br, 151 MHz, 298K): 148.5 (d, ²J_{C,F} 251 Hz, o-C₆F₅), 138.3 (d, ²J_{C,F} ~250 Hz, p-C₆F₅), 136.5 (d, ²J_{C,F} ~250 Hz, m-C₆F₅), 148.24, (NCN), 139.50 (C^{10,13}), 137.9 (C^{2,7}), 127.12 (C^{11,12}), 118.81 (CH^{1,8}), 114.18, 113.88 (N-CH), 113.95 (CH^{3,6}), 48.13, 47.95 (2 x CHMe₂), 39.8 (s, NCH₂SiMe₃), 37.1 (s, YCH₂SiMe₃ A), 34.4 (s, YCH₂SiMe₃ B), 36.48, 31.22 (2 x s, CMe₂), 36.31 (CMe₂), 24.34, 22.72, 21.93, 20.93 (4 x s, CHMe₂), 21.23 (s, C^{2,7}Me), 3.64 (s, YCH₂SiMe₃ A), 3.04 (s, YCH₂SiMe₃ B), -1.60 (s, NCH₂SiMe₃). Note: The CH₂SiMe₃ ¹³C NMR signals were not visible in the ¹³C{¹H} NMR spectrum, and were located from the 2D ¹H-¹³C HSQC and HMBC NMR spectra. ¹¹B{¹H} NMR (C₆D₅Br, 161 MHz, 298K): -16.17 (s, B(C₆F₅)₄). ¹⁹F NMR (C₆D₅Br, 470 MHz, 298K): -131.29 (s, o-F B(C₆F₅)₄).

Representative Procedure for in-situ Hydroamination using [(All₂)Y(CH₂SiMe₃)₂] (1) or [(All₂)Y(CH₂SiMe₃)₂] (1) / [CPh₃][B(C₆F₅)₄]: In the glovebox, a freshly prepared solution of the catalyst (**1** in C₆D₆ or **1**/[CPh₃][B(C₆F₅)₄] in C₆D₅Br) was added to a 1:1 mixture of the hydroamination substrate and ferrocene (an internal standard) at room temperature, to give a total volume of 0.8 mL. The amount of catalyst ranged from 1.5 to 6.4 μmol. Most reactions used 0.12 mmol of substrate, although

kinetic studies used 0.16 mmol. A portion of the resulting solution was immediately placed in a PTFE valved NMR tube, and the reaction was monitored at 24 °C by ¹H NMR spectroscopy.

Conflicts of interest

There are no conflicts to declare.

Acknowledgements

D.J.H.E thanks NSERC of Canada for a Discovery Grant. We are grateful to Charles J. Walsby at Simon Fraser University for advice regarding EPR spectroscopy.

Notes and references

† Reactions of **1** with B(C₆F₅)₃ or [HNMe₂Ph][B(C₆F₅)₄] in C₆D₅Br afforded complex mixtures of unidentified products, and were not pursued further. A reaction of **1** with [FeCp₂][B(C₆F₅)₄] in C₆D₅Br did not proceed to a substantial extent due to poor solubility of [FeCp₂][B(C₆F₅)₄] in this solvent. Nevertheless, an EPR signal was observed corresponding to the same paramagnetic species from the reaction of **1** with [CPh₃][B(C₆F₅)₄], and a very small amount of **3** was observed in the ¹H NMR spectrum.

‡ Reaction of scandium compound **2** with [CPh₃][B(C₆F₅)₄] in C₆D₅Br also generated a dark purple solution. However, the resulting ¹H NMR spectrum (Figure S44) was broad and featureless (between 20 and -25 °C), including signals for protons located in the plane of the ligand backbone (i.e. protons which would be unaffected by a fluxional process involving alkyl group migration between sites above and below the plane of the ligand backbone), indicating the absence of a soluble diamagnetic metal complex. The combination of **2** with [CPh₃][B(C₆F₅)₄] in C₆D₅Br was inactive for intramolecular hydroamination catalysis.

§ Other coupling schemes (where a(¹⁴N) ≈ a(¹H) and a(⁸⁹Y) ≈ 2 a(¹H)) could also give rise to a nonet, such as coupling to (a) 8 × ¹H, (b) 2 × ¹⁴N and 4 × ¹H, (c) 3 × ¹⁴N and 2 × ¹H, (d) 1 × ¹⁴N, 4 × ¹H and 1 × ⁸⁹Y, or (e) 2 × ¹⁴N, 2 × ¹H and 1 × ⁸⁹Y. However, a lack of significant coupling to ¹⁴N (option a) seems unlikely, and in options (b)-(e), the resulting peak integrations match less closely to the experimental spectrum.

- 1 E. Peris and R. H. Crabtree, *Chem. Soc. Rev.*, 2018, **47**, 1959.
- 2 C. E. Hayes and D. B. Leznoff, *Dalton Trans.*, 2012, **41**, 5743.
- 3 M. E. O'Reilly and A. S. Veige, *Chem. Soc. Rev.*, 2014, **43**, 6325.
- 4 C. A. Cruz, D. J. H. Emslie, L. E. Harrington, J. F. Britten and C. M. Robertson, *Organometallics*, 2007, **26**, 692.
- 5 C. A. Cruz, T. Chu, D. J. H. Emslie, H. A. Jenkins, L. E. Harrington and J. F. Britten, *J. Organomet. Chem.*, 2010, **695**, 2798.
- 6 C. A. Cruz, D. J. H. Emslie, H. A. Jenkins and J. F. Britten, *Dalton Trans.*, 2010, **39**, 6626.
- 7 B. Vidjayacoumar, S. Ilango, M. J. Ray, T. Chu, K. B. Kolpin, N. R. Andreychuk, C. A. Cruz, D. J. H. Emslie, H. A. Jenkins and J. F. Britten, *Dalton Trans.*, 2012, **41**, 8175.
- 8 N. R. Andreychuk, S. Ilango, B. Vidjayacoumar, D. J. H. Emslie and H. A. Jenkins, *Organometallics*, 2013, **32**, 1466.
- 9 N. R. Andreychuk, D. J. H. Emslie, H. A. Jenkins and J. F. Britten, *J. Organomet. Chem.*, 2018, **857**, 16.
- 10 C. A. Cruz, D. J. H. Emslie, L. E. Harrington and J. F. Britten, *Organometallics*, 2008, **27**, 15.
- 11 C. A. Cruz, D. J. H. Emslie, C. M. Robertson, L. E. Harrington, H. A. Jenkins and J. F. Britten, *Organometallics*, 2009, **28**, 1891.
- 12 N. R. Andreychuk, B. Vidjayacoumar, J. S. Price, S. Kervazo, C. A. Peeples, D. J. H. Emslie, V. Vallet, A. S. P. Gomes, F. Real, G.

- 13 Schreckenbach, P. W. Ayers, I. Vargas-Baca, H. A. Jenkins and J. F. Britten, *Chem. Sci.*, 2022, **13**, 13748.
- 14 K. S. A. Motolko, J. S. Price, D. J. H. Emslie, H. A. Jenkins and J. F. Britten, *Organometallics*, 2017, **36**, 3084.
- 15 K. S. A. Motolko, D. J. H. Emslie and H. A. Jenkins, *Organometallics*, 2017, **36**, 1601.
- 16 K. S. A. Motolko, D. J. H. Emslie and J. F. Britten, *RSC Adv.*, 2017, **7**, 27938.
- 17 R. M. Porter and A. A. Danopoulos, *Polyhedron*, 2006, **25**, 859.
- 18 N. R. Andreychuk, T. Dickie, D. J. H. Emslie and H. A. Jenkins, *Dalton Trans.*, 2018, **47**, 4866.
- 19 N. R. Andreychuk and D. J. H. Emslie, *Angew. Chem. Int. Ed.*, 2013, **52**, 1696.
- 20 J. Hicks, P. Vasko, J. M. Goicoechea and S. Aldridge, *Nature*, 2018, **557**, 92.
- 21 J. Hicks, P. Vasko, J. M. Goicoechea and S. Aldridge, *J. Am. Chem. Soc.*, 2019, **141**, 11000.
- 22 J. Hicks, P. Vasko, A. Heilmann, J. M. Goicoechea and S. Aldridge, *Angew. Chem. Int. Ed.*, 2020, **59**, 20376.
- 23 M. M. D. Roy, A. Heilmann, M. A. Ellwanger and S. Aldridge, *Angew. Chem. Int. Ed.*, 2021, **60**, 26550.
- 24 A. Heilmann, M. M. D. Roy, A. E. Crumpton, L. P. Griffin, J. Hicks, J. M. Goicoechea and S. Aldridge, *J. Am. Chem. Soc.*, 2022, **144**, 12942.
- 25 M. M. D. Roy, J. Hicks, P. Vasko, A. Heilmann, A. M. Baston, J. M. Goicoechea and S. Aldridge, *Angew. Chem. Int. Ed.*, 2021, **60**, 22301.
- 26 A. Heilmann, J. Hicks, P. Vasko, J. M. Goicoechea and S. Aldridge, *Angew. Chem. Int. Ed.*, 2020, **59**, 4897.
- 27 J. Hicks, A. Heilmann, P. Vasko, J. M. Goicoechea and S. Aldridge, *Angew. Chem. Int. Ed.*, 2019, **58**, 17265.
- 28 J. Hicks, A. Mansikkamaki, P. Vasko, J. M. Goicoechea and S. Aldridge, *Nat. Chem.*, 2019, **11**, 237.
- 29 C. McManus, J. Hicks, X. L. Cui, L. L. Zhao, G. Frenking, J. M. Goicoechea and S. Aldridge, *Chem. Sci.*, 2021, **12**, 13458.
- 30 C. McManus, A. E. Crumpton and S. Aldridge, *Chem. Commun.*, 2022, **58**, 8274.
- 31 J. S. McMullen, A. J. Edwards and J. Hicks, *Dalton Trans.*, 2021, **50**, 8685.
- 32 F. Kramer, M. S. Luff, U. Radius, F. Weigend and F. Breher, *Eur. J. Inorg. Chem.*, 2021, **2021**, 3591.
- 33 L. F. Lim, M. Judd, P. Vasko, M. G. Gardiner, D. A. Pantazis, N. Cox and J. Hicks, *Angew. Chem. Int. Ed.*, 2022, **61**, e202201248.
- 34 A. Nicolay, M. S. Ziegler, L. Rochlitz and T. D. Tilley, *Polyhedron*, 2020, **180**, 114420.
- 35 E. W. Y. Wong and D. J. H. Emslie, *Dalton Trans.*, 2015, **44**, 11601.
- 36 X. Wu and M. Tamm, *Coord. Chem. Rev.*, 2014, **260**, 116.
- 37 D. Petrovic, T. Bannenberg, S. Randall, P. G. Jones and M. Tamm, *Dalton Trans.*, 2007, 2812.
- 38 T. K. Panda, C. G. Hrib, P. G. Jones, J. Jenter, P. W. Roesky and M. Tamm, *Eur. J. Inorg. Chem.*, 2008, 4270.
- 39 D. Petrovic, L. M. R. Hill, P. G. Jones, W. B. Tolman and M. Tamm, *Dalton Trans.*, 2008, 887.
- 40 T. K. Panda, D. Petrovic, T. Bannenberg, C. G. Hrib, P. G. Jones and M. Tamm, *Inorg. Chim. Acta*, 2008, **361**, 2236.
- 41 D. Petrovic, C. G. Hrib, S. Randall, P. G. Jones and M. Tamm, *Organometallics*, 2008, **27**, 778.
- 42 S. Randall, P. G. Jones and M. Tamm, *Organometallics*, 2008, **27**, 3232.
- 43 S. A. Filimon, C. G. Hrib, S. Randall, I. Neda, P. G. Jones and M. Tamm, *Z. Anorg. Allg. Chem.*, 2010, **636**, 691.
- 44 T. Gloge, K. Jess, T. Bannenberg, P. G. Jones, N. Langenscheidt-Dabringhausen, A. Salzer and M. Tamm, *Dalton Trans.*, 2015, **44**, 11717.
- 45 K. Jess, D. Baabe, T. Bannenberg, K. Brandhorst, M. Freytag, P. G. Jones and M. Tamm, *Inorg. Chem.*, 2015, **54**, 12032.

- 45 J. Bogojeski, J. Volbeda, Z. D. Bugarcic, M. Freytag and M. Tamm, *New J. Chem.*, 2016, **40**, 4818.
- 46 K. Jess, V. Derdau, R. Weck, J. Atzrodt, M. Freytag, P. G. Jones and M. Tamm, *Adv. Synth. Catal.*, 2017, **359**, 629.
- 47 S. Dastgir and G. G. Lavoie, *Dalton Trans.*, 2010, **39**, 6943.
- 48 T. G. Larocque, S. Dastgir and G. G. Lavoie, *Organometallics*, 2013, **32**, 4314.
- 49 M. Y. Li, X. Shu, Z. G. Cai and M. S. Eisen, *Organometallics*, 2018, **37**, 1172.
- 50 A. McSkimming and D. L. M. Suess, *Inorg. Chem.*, 2018, **57**, 14904.
- 51 S. T. Xu, J. X. Wang, J. J. Zhai, F. Wang, L. Pan and X. C. Shi, *Organometallics*, 2021, **40**, 3323.
- 52 D. Maiti, B. P. Fors, J. L. Henderson, Y. Nakamura and S. L. Buchwald, *Chem. Sci.*, 2011, **2**, 57.
- 53 Based on a search of the Cambridge Structural Database, >90% of the Y–C distances to terminal CH₂SiMe₃ ligands lie between 2.36 and 2.47 Å.
- 54 R. D. Shannon, *Acta Cryst.*, 1976, **A32**, 751.
- 55 R. A. Kunetskiy, S. M. Polyakova, J. Vavrik, I. Cisarova, J. Saame, E. R. Nerut, I. Koppel, I. A. Koppel, A. Kutt, I. Leito and I. M. Lyapkalo, *Chem. Eur. J.*, 2012, **18**, 3621.
- 56 S. A. Filimon, D. Petrovic, J. Volbeda, T. Bannenberg, P. G. Jones, C. G. F. von Richthofen, T. Glaser and M. Tamm, *Eur. J. Inorg. Chem.*, 2014, 5997.
- 57 S. Hong and T. J. Marks, *Acc. Chem. Res.*, 2004, **37**, 673.
- 58 T. E. Müller, K. C. Hultsch, M. Yus, F. Foubelo and M. Tada, *Chem. Rev.*, 2008, **108**, 3795.
- 59 A. L. Reznichenko and K. C. Hultsch, *Top. Organomet. Chem.*, 2013, **43**, 51.
- 60 J. Hannedouche and E. Schulz, *Organometallics*, 2018, **37**, 4313.
- 61 P. Colonna, S. Bezenine, R. Gil and J. Hannedouche, *Adv. Synth. Catal.*, 2020, **362**, 1550.
- 62 S. Bambirra, H. Tsurugi, D. van Leusen and B. Hessen, *Dalton Trans.*, 2006, 1157.
- 63 R. M. Beesley, C. K. Ingold and J. F. Thorpe, *J. Chem. Soc.*, 1915, **107**, 1080.
- 64 S. Bambirra, A. Meetsma and B. Hessen, *Organometallics*, 2006, **25**, 3454.
- 65 S. Z. Ge, A. Meetsma and B. Hessen, *Organometallics*, 2008, **27**, 5339.
- 66 F. Lauterwasser, P. G. Hayes, S. Brase, W. E. Piers and L. L. Schafer, *Organometallics*, 2004, **23**, 2234.
- 67 D. M. Lyubov, L. Luconi, A. Rossin, G. Tuci, A. V. Cherkasov, G. K. Fukin, G. Giambastiani and A. A. Trifonov, *Chem. Eur. J.*, 2014, **20**, 3487.
- 68 A. Rajput, A. K. Sharma, S. K. Barman, A. Saha and R. Mukherjee, *Coord. Chem. Rev.*, 2020, **414**.
- 69 V. Lyaskovskyy and B. de Bruin, *Acs Catalysis*, 2012, **2**, 270.
- 70 W. Kaim, *Inorg. Chem.*, 2011, **50**, 9752.
- 71 L. A. Casper, L. Wursthorn, M. Geppert, P. Roser, M. Linseis, M. Drescher and R. F. Winter, *Organometallics*, 2020, **39**, 3275.
- 72 J. Underhill, E. S. Yang, T. Schmidt-Rantsch, W. K. Myers, J. M. Goicoechea and J. Abbenseth, *Chem. Eur. J.*, 2022, **29**, e202203266.
- 73 P. D. Bolton, E. Clot, N. Adams, S. R. Dubberley, A. R. Cowley and P. Mountford, *Organometallics*, 2006, **25**, 2806.
- 74 C. Y. Wang, Y. Zheng, H. H. Huo, P. Rose, L. L. Zhang, K. Harms, G. Hilt and E. Meggers, *Chem. Eur. J.*, 2015, **21**, 7355.
- 75 D. Alberti and K.-R. Pörschke, *Organometallics*, 2004, **23**, 1459.
- 76 R. G. Belli, V. C. Tafuri, M. V. Joannou and C. C. Roberts, *Acs Catalysis*, 2022, **12**, 3094.
- 77 R. G. Belli, V. C. Tafuri and C. C. Roberts, *Acs Catalysis*, 2022, **12**, 9430.
- 78 R. F. Jordan, R. E. Lapointe, C. S. Bajgur, S. F. Echols and R. Willett, *J. Am. Chem. Soc.*, 1987, **109**, 4111.
- 79 S. L. Borkowsky, R. F. Jordan and G. D. Hinch, *Organometallics*, 1991, **10**, 1268.
- 80 S. L. Borkowsky, N. C. Baenziger and R. F. Jordan, *Organometallics*, 1993, **12**, 486.
- 81 M. R. Haneline and A. F. Heyduk, *J. Am. Chem. Soc.*, 2006, **128**, 8410.
- 82 J. C. Hayes and N. J. Cooper, *J. Am. Chem. Soc.*, 1982, **104**, 5570.
- 83 R. C. Klet, D. M. Kaphan, C. Liu, C. Yang, A. J. Kropft, F. A. Perras, M. Pruski, A. S. Hock and M. Delferro, *J. Am. Chem. Soc.*, 2018, **140**, 6308.
- 84 M. Sharma, H. S. Yameen, B. Tumanskii, S. A. Filimon, M. Tamm and M. S. Eisen, *J. Am. Chem. Soc.*, 2012, **134**, 17234.
- 85 T. Y. Cheng, D. J. Szalda, J. Zhang and R. M. Bullock, *Inorg. Chem.*, 2006, **45**, 4712.
- 86 O. B. Ryan, K. T. Smith and M. Tilset, *J. Organomet. Chem.*, 1991, **421**, 315.
- 87 F. Estler, G. Eickerling, E. Herdtweck and R. Anwender, *Organometallics*, 2003, **22**, 1212.
- 88 G. L. Cai, Y. D. Huang, T. T. Du, S. W. Zhang, B. Yao and X. F. Li, *Chem. Commun.*, 2016, **52**, 5425.
- 89 Method A in J. J. Adams, N. Arulsamy, B. P. Sullivan, D. M. Roddick, A. Ne-Uberger and R. H. Schmehl, *Inorg. Chem.*, 2015, **54**, 11136.
- 90 M. Tamm, D. Petrovic, S. Randoll, S. Beer, T. Bannenberg, P. G. Jones and O. Grunenberg, *Organic & Biomolecular Chemistry*, 2007, **5**, 523.
- 91 M. R. Crimmin, M. Arrowsmith, A. G. M. Barrett, I. J. Casely, M. S. Hill and P. A. Procopiou, *J. Am. Chem. Soc.*, 2009, **131**, 9670.
- 92 Thomas Casey (2023). cwEPR (https://www.mathworks.com/matlabcentral/fileexchange/7329_2-cwepr), MATLAB Central File Exchange. Retrieved February 2023.
- 93 S. Stoll and A. Schweiger, *Journal of Magnetic Resonance*, 2006, **178**, 42.